Nuclear Instruments and Methods in Physics Research B 297 (2013) 29–34

Contents lists available at SciVerse ScienceDirect

Nuclear Instruments and Methods in Physics Research B

journal homepage: www.elsevier.com/locate/nimb

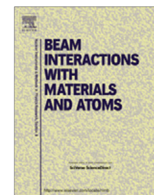


# Annealing temperature effects on the magnetic properties and induced defects in C/N/O implanted MgO

Qiang Li [a], Bonian Ye [b], Yingping Hao [b], Jiandang Liu [a], Wei Kong [a], Bangjiao Ye [a,*]

[a] State Key Laboratory of Particle Detection and Electronics, Department of Modern Physics, University of Science and Technology of China, Hefei 230026, PR China
[b] Key Laboratory of Nuclear Analysis Techniques, Shanghai Institute of Applied Physics, Chinese Academy of Sciences, Shanghai 201800, PR China

ARTICLE INFO

*Article history:*
Received 13 October 2012
Received in revised form 19 December 2012
Available online 27 December 2012

*Keywords:*
Ions implantation
Diluted magnetic semiconductors
Vacancy defects
Positron annihilation spectroscopy

ABSTRACT

Virgin MgO single crystals were implanted with 70 keV C/N/O ions at room temperature to a dose of $2 \times 10^{17}/cm^2$. After implantation the samples showed room temperature hysteresis in magnetization loops. The annealing effects on the magnetic properties and induced defects of these samples were determined by vibrating sample magnetometer and positron annihilation spectroscopy, respectively. The experimental results indicate that ferromagnetism can be introduced to MgO single crystals by doping with C, N or introduction of Mg related vacancy defects. However, the Mg vacancies coexistence with C or N ions in the C-/N-implanted samples may play a negative role in magnetic performance in these MgO samples. The rapid increase of magnetic moment in O-implanted sample is attributed to the formation of new type of vacancy defects.

© 2013 Elsevier B.V. All rights reserved.

## 1. Introduction

Diluted magnetic semiconductors (DMSs) have attracted considerable attention because of their potential use in spintronic devices [1]. Although the origin of magnetism has not been established clearly, transition-metal (TM) doping proved to be a feasible method to obtain room temperature ferromagnetism (RTFM) in doped semiconductors [2–5]. In recent years, RTFM has also been found in series of non-TM doped metallic oxides such as C-doped ZnO, N-doped MgO, and pure MgO films [6–8]. However, the observed ferromagnetism is always rather weak and many controversial results also have been reported [9–12]. For example, Araujo et al. observed that ferromagnetism in MgO films was mediated by cation vacancies [8]. However, a recent report on MgO nanosheets attributed low-temperature ferromagnetism to unpaired electrons trapped at oxygen vacancies [12].

Ion implantation as an effective way of doping has been used to introduce ferromagnetism into metal oxides [13–15]. However, a certain amount of defects is also introduced in materials after ion implantation. These defects will inevitably affect the ferromagnetic performance of implanted samples. For TM-doped materials, it was demonstrated that defects induced carrier plays an important role in mediating the ferromagnetic interactions [16,17]. Defect induced magnetism (DIM) was also used to explain the RTFM in oxide semiconductors. Therefore, the effect of induced defects on magnetism should be determined in non-TM implanted samples. Meanwhile, ferromagnetic impurities in raw samples should be characterized with the best available methods in this research field, which has been carefully presented in a recent study [18].

In the present work, a detailed study of the magnetic properties and induced defects of C-/N-/O-implanted MgO single crystals are reported. After implantation the samples were annealed at temperatures from RT to 1200 °C. Before and after each annealing step magnetic properties and defect depth profiles were determined by vibrating sample magnetometer (VSM) and positron annihilation spectroscopy, respectively. Ferromagnetic impurities in the samples were characterized by inductively coupled plasma emission spectroscopy (ICP-ES). In C-/N-implanted samples, the strong dependence of magnetic properties on implanted C or N ions instead of on the defects was detected by VSM measurements of annealed samples. The depth profiles of C ions before and after annealing were measured by secondary ion mass spectrometry (SIMS). The C or N ions effect on annealing behavior of induced defects was also observed.

## 2. Experiment details

MgO single crystals (0.5 mm thickness) were purchased from the Chinese Academy of Sciences (Shanghai). They were cut into a size of 6 × 8 mm and then decontaminated in ultrasonic acetone for 10 min. The ICP-ES analysis showed traces of Fe, Co, Ni, Mn, Cr, and Ca impurities in raw wafers. From the ICP-ES analyses, the maximum amount of magnetic impurities in wafers was found to be less than 10 ppm for any kind of element except of Ca. Ca impurity peak can be seen in XRF measurement and the content given

* Corresponding author. Tel.: +86 0551 3607404.
*E-mail address:* bjye@ustc.edu.cn (B. Ye).

0168-583X/$ - see front matter © 2013 Elsevier B.V. All rights reserved.
http://dx.doi.org/10.1016/j.nimb.2012.12.012

by ICP-ES analyses was 1.16 mg/g. Ca impurities are presumably diamagnetic and do not contribute to the paramagnetic response [18]. Ion-implantation was performed using a 100 keV Electromagnetic Isotope Separator at the Shanghai Institute of Applied Physics (SIAP). C, N, and O-ions at 70 keV were implanted into the polished surface of different MgO crystals at room temperature to a dose of $2 \times 10^{17}/cm^2$. The implantation layer range by the SRIM simulation was approximately from 50 nm to 160 nm. XRD measurements showed considerable broadening of diffraction peak, which indicate that lattice defects are introduced in the implanted layers. After ion-implantation, samples were isochronally annealed at different temperatures (400, 800 and 1200 °C) for 20 min in air. Before and after each annealing step room-temperature magnetic properties were measured using the VSM with an accuracy of $10^{-7}$ emu. Plastic tweezers were used during the measurement to avoid contact with magnetic impurities. The non-implanted MgO substrates exhibit linear background diamagnetic behavior, which were subtracted for all the displayed data.

## 3. Results and discussion

Fig. 1 shows the VSM results of field-dependent magnetization curves at 300 K. For the as-implanted samples, room-temperature FM were realized among all samples and well-defined hysteresis loops also could be observed in enlarged low field region. The saturation magnetization for the O-implanted sample is significantly weaker than that of C- or N-implanted samples. The comparisons of as-implanted and annealed M-H curves are shown in the different pictures for each sample. As shown in Fig. 1(a), a reduction of almost 3/4 of the magnetization is observed after the sample annealed at 400 °C. The sample annealed at 800 °C shows a further reduction of the magnetization. A linear response of M-H curve is observed in insert, which indicating a paramagnetic behavior. It is interesting to note that there is a weak increase in the magnetization after the sample annealed at 1200 °C. Well-defined retrieve of ferromagnetism can be found in the insert. For the N-implanted sample in Fig. 1(b), the ferromagnetism monotonously decreases with the increase annealing temperature. The saturation magnetization slightly decreases with the annealing temperature at 400 °C and then shows a rapid decline at an annealing temperature of 800 °C. Increasing the annealing temperature further to 1200 °C, as insert shows, the hysteresis disappear and the room-temperature FM was almost removed. Similar annealing effects were also obtained for the O-implanted sample annealed at 400 and 800 °C. Fig. 1(c) shows the magnetization of O-implanted sample gradually decreases with the annealing temperature up to 400 and 800 °C. It was also observed in previous report of pure MgO films [19]. Noteworthy, very different results were obtained when the sample annealed at 1200 °C. A rapid increase of magnetization, exceed the initial value was observed after this annealing process. The interesting result clearly indicates that the ferromagnetism in O-implanted MgO is strongly affected by evolution of induced defects, which may very different from the case of C- or N-implanted samples.

The generation and annealing behavior of defects were detected by positron annihilation spectroscopy, which was proved to be an effective tool for study of defects in materials [20]. Positrons have a high affinity to be captured by vacancy defects, which results in a narrowing of the 511 keV annihilation peak compared to bulk annihilation. The Doppler broadening of the annihilation peak was characterized by the line-shape parameters S and W, which defined as a fraction of counts in the central area and the wing area of the peak, respectively [21]. Thus, positrons trapped in vacancy defects will result in an increase in S and a decrease in W. Each defect type exhibits its own specific S and W parameter. Therefore, S

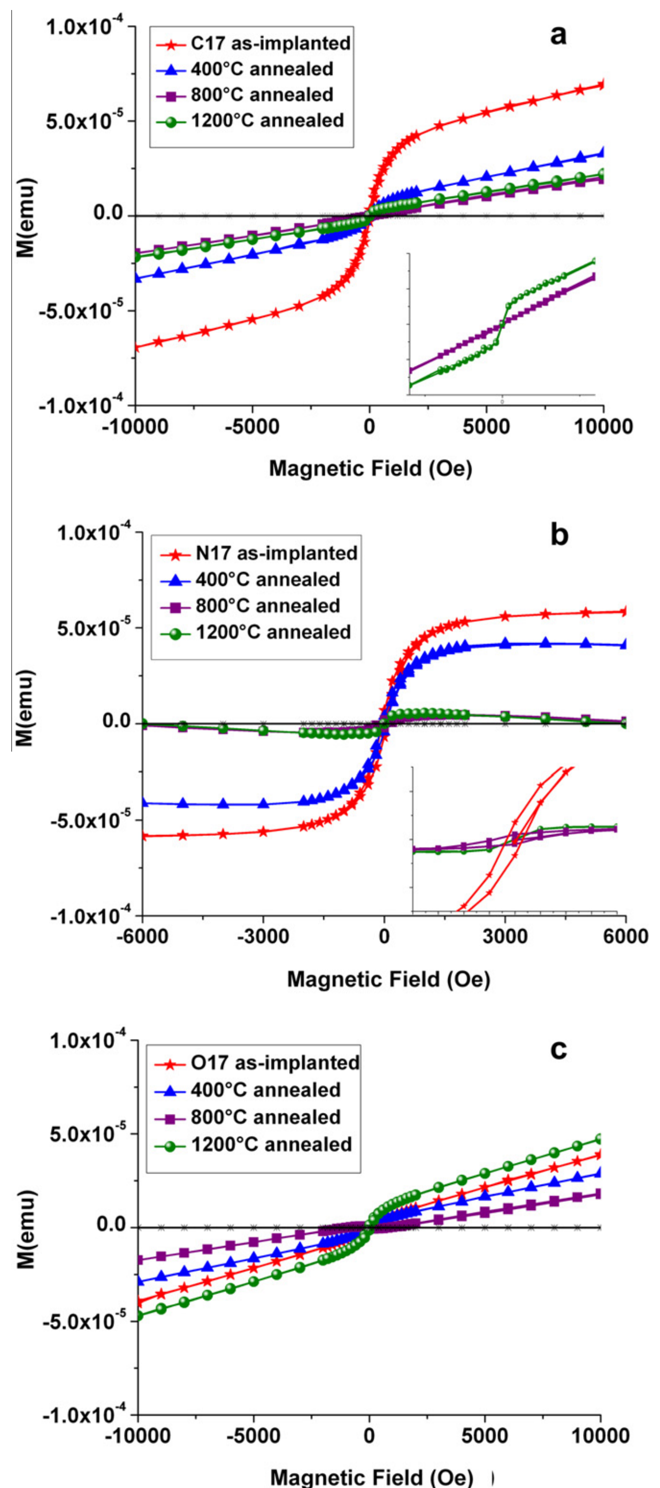


**Fig. 1.** Magnetization versus magnetic field measured at room temperature for the as-implanted sample, 400, 800 and 1200 °C annealed samples after different ions implanted MgO with implantation dose of $2 \times 10^{17}$ ions $cm^{-2}$: (a) C-implantation; (b) N-implantation and (c) O-implantation. Insert in pattern (a) shows apparent comparison of C-implanted sample annealed at 1200 and 800 °C in low magnetic field. The same case of N-implanted sample is shown in insert of pattern (b).

depends linearly on W will observed if only single type of defects was introduced [22]. Doppler-broadening experiments were carried out using a beam of mono-energetic positrons with energies changing from 0.5 to 18 keV. Normalized S parameter as a function of positron implantation energy was used to analyze the defects in

samples. The results are shown in Fig. 2. Based on VEPFIT analyses, the plots were divided into three layers. In layer I, positron energy range of 0.25–2 keV corresponds to annihilation at the surface of samples, which exhibit high S parameters due to the surface effects. In layer II, energy range between 2 and 7.5 keV is regarded as the characteristic of ion-implanted layer. Finally, positrons annihilate mainly in the MgO substrate while the incident energy above 7.5 keV, leading to over-lapping of the plots in layer III. The mean depth of positron penetration corresponding to the incident energy is indicated in the top axis. In the virgin MgO, S parameter decreases rapidly to the bulk value at $E < 3$ keV, and the layer II does not exist in this sample. In the as-implanted samples, the increases of S parameters in their injection layer clearly show the emergence of vacancy defects after implantation. However, different annealing behavior of these defects was observed in the samples. For C-implanted sample in Fig. 2(a), 400 °C annealing did not exhibit significant change of S parameters compared with that of as-implanted sample. The S parameters in injection layer show apparent increase with annealing temperature at 800 °C and then decreases to initial value after further annealing at 1200 °C. Fig. 2(b) shows the annealing results of N-implanted sample. The S parameters rapid increase after sample annealed at 400 °C and then shows further increases at an annealing temperature of 800 °C. The similar results also have been observed in He-implanted MgO and N-implanted ZnO [23–24]. For the sample annealed at 1200 °C, the S parameters rapidly decreases below to the as-implanted value. Differently, as shown in Fig. 2(c), the S parameters monotonously decreases with the increase annealing temperature are observed in O-implanted sample. These results indicate that annealing behavior of defects can be strongly influenced by the presence of impurity ions in MgO samples.

The evolution of both vacancy size and vacancy density may cause the change of S-parameters [24]. Thus, in order to check the change of vacancy type we performed S–W analysis for all the annealed samples as shown in Fig. 3. The surface points corresponding to positron energy below 2 keV were removed from all the S–W data. The straight line of S–W data were observed in both C- and N-implanted samples as shown in Fig. 3(a) and (b), which

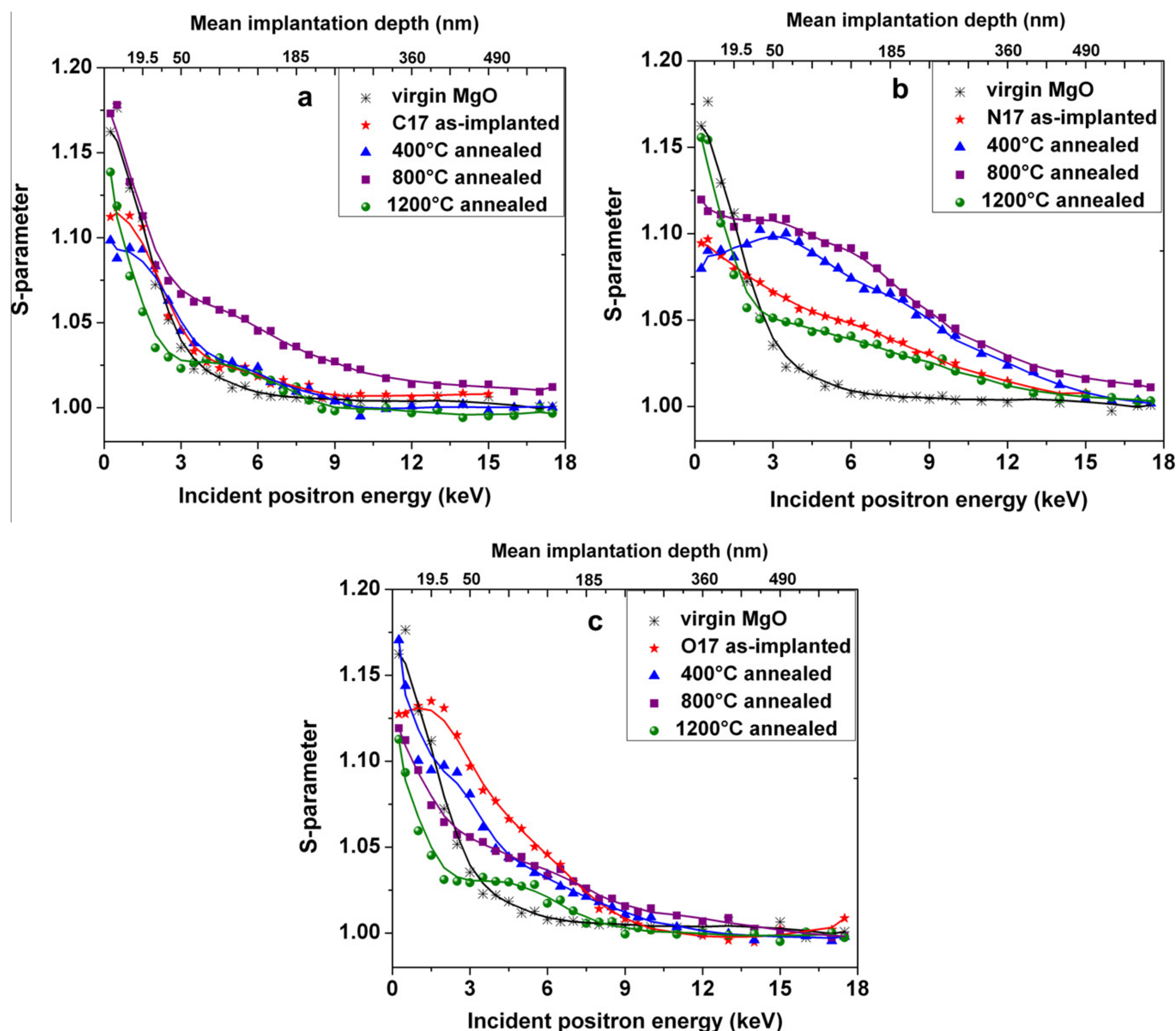


**Fig. 2.** The S-parameter as a function of positron implantation energy for (a) C-, (b) N-, and (c) O-implanted MgO crystals. The curves are shown for the as implanted case and for the samples annealed at 400, 800, and 1200 °C. The mean depth of positron penetration corresponding to the incident energy is indicated in the top axis. Lines through the data are obtained from the VEPFIT analyses.

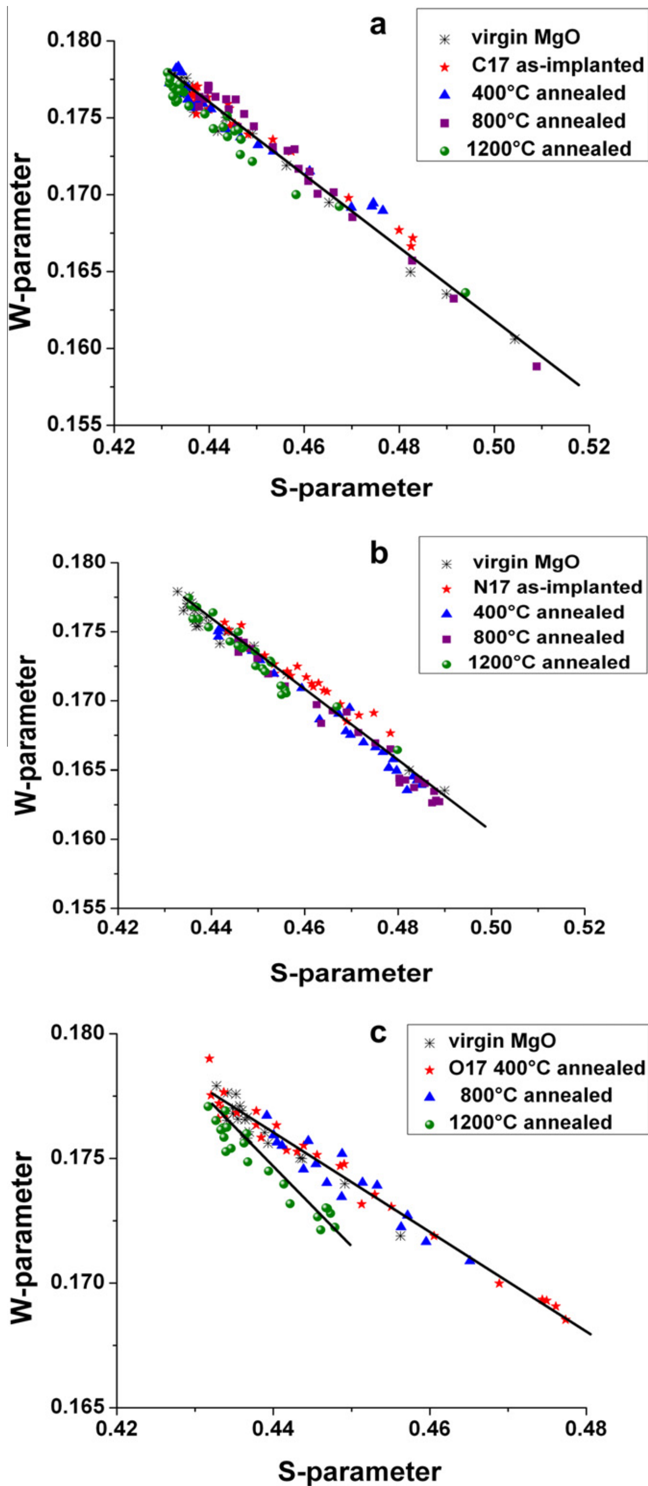


**Fig. 3.** The dependence of W and S parameters for (a) C-, (b) N-, and (c) O-implanted MgO samples and for the samples annealed at selected temperature. The surface points corresponding to positron energy below 2 keV have been removed. The lines are drawn to guide the eye.

indicates that only one type of defects exist in these samples after implantation. For the samples annealed at temperatures from 400 °C to 1200 °C, the S–W plots show nearly linear variation and overlap the initial data of as-implantation. This means that the change of S parameters in these samples is mainly caused by vacancy density changes, but not the vacancy type. Cation vacancies as dominant positron trapping defects generally exist in materials. Thus, the single type of defects in layer II of these samples is considered mainly Mg related vacancies. However, as shown in Fig. 3(c), the only deviation of the linear S–W data was observed which corresponds to the O-implanted sample annealing at 1200 °C. It is indicates that new type of vacancy defects was formed in the sample after this annealing stage. This may far from the situation of C- or N-implantation.

For C-implanted sample, it's obvious that both defect type and density have no significant change after annealed at 400 °C. However, a rapid decrease of magnetization was observed at the stage. It is revealed that most of the room temperature ferromagnetism in C-implanted sample is attributed to the presence of C ions instead of to the induced Mg vacancies. The decrease of magnetization might interpret as the annealing-induced migration of C ions in MgO substrate. After processing at high temperatures, vacancies are more likely to migrate and agglomerate into vacancy clusters, which may be responsible for the increase in S parameters after 800 °C annealing [24]. Moreover, C impurities release form substitutional site may also cause the increase of S parameters. A further decrease of magnetization was observed at this stage. S parameters drop to the value of as-implanted level at 1200 °C annealing. It is indicates that some vacancies are recovered after this high-temperature annealing but not all of them are removed from the sample. The corresponding M-H curve shows an interesting retrieve in magnetization while the magnetization is far from reach the initial value of as-implantation. On the one hand, this means that the Mg vacancies in C-implanted sample may play a negative role in magnetic performance, which is different from defect-induced RTFM in pure MgO. It is unwise to superimpose that Mg vacancies induced ferromagnetism on observed RTFM because the co-presence of C impurities may involve complex interaction. From a theoretical point of view, vacancy defects as lattice distortion may promotes the localization of the doping hole, thus the long range magnetic coupling between impurities was suppressed [9]. Actually, the interaction performance between Mg vacancies and C impurities should variably depend on their relative site in materials. On the other hand, density variation of Mg vacancies may not be the main reason for the decrease of magnetization in this sample. Therefore, the main reason might be due to the carbon impurities. Fig. 4 displays the depth profiles of C impurities in MgO crystal after as-implantation and annealing at 1200 °C analyzed by SIMS. Before

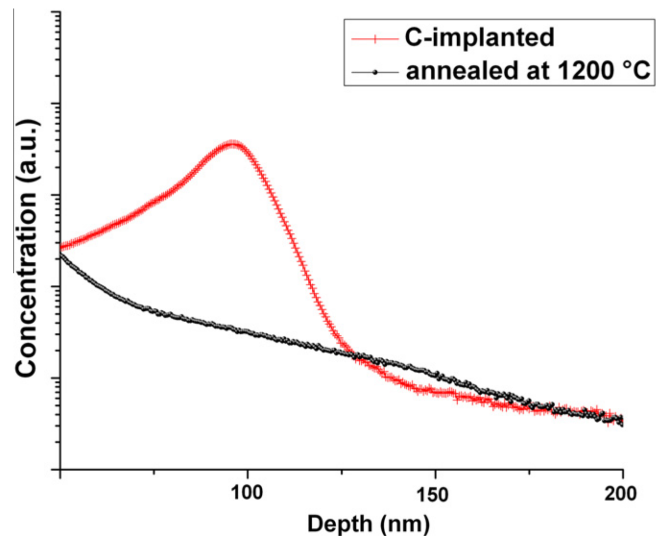


**Fig. 4.** SIMS depth profiles of C-implanted MgO and annealed at 1200 °C.

annealing, the injection-induced density peak of C ions is observed at approximately 100 nm and the distribution layer thickness is about 90 nm, which in roughly agree with the SRIM simulation. Annealing-induced diffusion of C impurities was observed since the injection peak disappeared after 1200 °C annealing, which is considered as the main cause of the magnetization decrease. It's further confirmed that most of the RTFM in this sample should due to the C impurities. The significant increase of S-parameters in N-implanted sample after 400 °C annealing is greater than that of C-implanted sample. The S-parameters even reaches to 1.10 after sample annealed at 800 °C. It seems that some larger trapping centers appear. However, there is no standard value of S-parameter for positrons trapping at certain vacancy type. The saturated S-parameter of certain vacancy type may affected by selected channel numbers of acquisition module or other measuring factors. Thus, inconsistent value of S may be given in different reports [24,25]. Based on the linear variation of S–W plots, we would rather believe that the relative large S is still due to the increase of vacancy density. Previous reports based on calculation have shown that the formation energy of $V_O$ in MgO is about 10.6 eV; the energy cost of removing N atom from cavity is only about 6.2 eV [26]. It means that releasing N from substitution site into interstitial situation is a thermodynamically favorable process. On the other hand, substitutional N impurities which near the vacancies may involve in interaction to form defect complexes, which can also cause the increase in S-parameters [24]. The nitrogen-related vacancy complexes could reduce the ferromagnetic correlation between localized moments. As the ionic radius of N (0.013 nm) is much smaller than that of C (0.26 nm (Ref. [15]), covalent radius of C is 0.077 nm), the N impurities will more easily to migrate at certain annealing temperature. So a larger change of S-parameters and a faster decline of RTFM were observed in N-implanted sample. After annealing at 1200 °C, most of Mg vacancies were recovered but no retrieve of ferromagnetism was found. This might consider as the diffusion of N impurities is more serious than that of C impurities after annealing. Thus the N-induced magnetism no longer can be regained by further annealing at 1200 °C, although the vacancy complexes density was reduced below to the initial level of as-implantation. For the O-implantation, there are no impurity elements introduced in the sample. The close correlation between ferromagnetism and Mg vacancies density was observed in the annealing process. The magnetism decrease after annealing at 400 °C and 800 °C is due to recovery-induced decease of Mg vacancy concentration. After annealing at 1200 °C the sample shows interesting results that the magnetism rapidly increase but the S-parameters show a further decline. The S–W plot indicates that a new type of vacancy defects was formed at this stage. Considering the agglomeration of Mg vacancies, it could be believed that the agglomeration and recovery of Mg vacancies simultaneously occur during the annealing process. In 800 °C annealing stage, the slight increase of S at positron energy above 5 keV might give a hint for the agglomeration of Mg vacancies. At the temperature of 1200 °C, some Mg vacancies are merged into larger cavity formation, which is thought to be Mg divacancies or trivacancies. However, there's no direct evidence from our experiments on the type of new defects. Further confirmation of the defect type could be implemented by positron lifetime spectra, which is proved to be an effective tool and only apply to bulk samples. The further decrease of S in this stage may duo to the low concentration of new vacancies. Merger process might be inhibited by the existence of the C or N impurities in the other two samples. Calculated magnetic moment of Mg monovacancy after lattice relaxation is 1.51 μB [27]. Our experimental results are much smaller than this value. Long range magnetic coupling between moments has been proved to depend on the density-related distance of $V_{Mg}$–$V_{Mg}$. It means that not all the Mg vacancies contribute to the observed RTFM. As the magnetic moments of Mg divacancies (3.24 μB) and trivacancies (4.70 μB) are much larger than that of Mg vacancies, it is found that the new type of defects is more conducive to formation of obvious RTFM in MgO crystals [27]. The sharp increase of magnetism indicates more Mg vacancies were involved in the magnetic coupling in this case, although total vacancy concentration was decreased.

## 4. Conclusion

In conclusion, we have observed room temperature ferromagnetism in C-, N-, and O-implanted MgO crystals. The annealing behavior of magnetism and induced defects indicate that most of the ferromagnetism in C- and N-implanted samples should be attributed to the injected impurities. Mg vacancies as the origin of RTFM were also observed in O-implanted sample. However, the Mg vacancies in C- and N-implanted samples might involve in complex interaction with the injected ions, thus reducing the ferromagnetic performance of magnetic moment in the samples. The annealing effect of Mg vacancies can be strongly affected by the injected impurity ions. The new type of defects appear in the O-implanted sample are responsible for the rapid increase of magnetic moment after 1200 °C annealing.

## Acknowledgments

The authors are grateful for financial support from the State Key Program of National Natural Science of China (Grant No. 10835006) and 211 project of Ministry of Education of China.

## References

[1] S.A. Wolf, D.D. Awschalom, R.A. Buhrman, J.M. Daughton, S. VonMolnar, M.L. Roukes, A.Y. Chtochelkanova, D.M. Treger, Science 294 (2001) 1488.
[2] Hoa Hong Nguyen, Joe Sakai, W. Prellier, Awatef Hassini, Antoine Ruyter, François Gervais, Phys. Rev. B 70 (2004) 195204.
[3] Y.W. Heo, M.P. Ivill, K. Ip, D.P. Norton, S.J. Pearton, J.G. Kelly, R. Rairigh, A.F. Hebard, T. Steiner, Appl. Phys. Lett. 84 (2004) 2292.
[4] K.A. Griffin, A.B. Pakhomov, C.M. Wang, S.M. Heald, Kannan M. Krishnan, Phys. Rev. Lett. 94 (2005) 157204.
[5] R.P. Borges, J.V. Pinto, R.C. da Silva, A.P. Goncalves, M.M. Cruz, M. Godinho, J. Magn. Magn. Mater. 316 (2007) e191–e194.
[6] H. Pan, J.B. Yi, L. Shen, R.Q. Wu, J.H. Yang, J.Y. Lin, Y.P. Feng, J. Ding, L.H. Van, J.H. Yin, Phys. Rev. Lett. 99 (2007) 127201.
[7] Liu Chun-Ming, Gu Hai-Quan, Xiang Xia, Zhang Yan, Jiang Yong, Chen Men, Zu Xiao-Tao, Chin. Phys. B 20 4 (2011) 047505.
[8] C. Moyses Araujo, Mukes Kapilashrami, Xu Jun, O.D. Jayakumar, Sandeep Nagar, Yan Wu, Cecilia Århammar, Börje Johansson, Lyubov Belova, Rajeev Ahuja, Gillian A. Gehring, K.V. Rao, Appl. Phys. Lett. 96 (2010) 232505.
[9] A. Droghetti, S. Sanvito, Appl. Phys. Lett. 94 (2009) 252505.
[10] Wu Hua, Alessandro Stroppa, Sung Sakong, Silvia Picozzi, Matthias Scheffler, Peter Kratzer, Phys. Rev. Lett. 105 (2010) 267203.
[11] Nitesh Kumar, D. Sanyal, A. Sundaresan, Chemical, Phys. Lett. 477 (2009).
[12] Ben M. Maoz, Einat Tirosh, Maya Bar Sadan, Gil Markovich, Phys. Rev. B 83 (2011) 161201. R.
[13] Zhongquan Mao, Zhenhui He, Dihu Chen, W.Y. Cheung, S.P. Wong, Solid State Commun. 142 (2007) 329–332.
[14] M. Bolduc, C. Awo-Affouda, A. Stollenwerk, M.B. Huang, F.G. Ramos, G. Agnello, V.P. LaBella, Phys. Rev. B 71 (2005) 033302.
[15] Shengqiang Zhou, Qingyu Xu, Kay Potzger, Georg Talut, Rainer Grötzschel, Jürgen Fassbender, Mykola Vinnichenko, Jörg Grenzer, Manfred Helm, Holger Hochmuth, Michael Lorenz, Marius Grundmann, Heidemarie Schmidt, Appl. Phys. Lett. 93 (2008) 232507.
[16] Nicola A. Spaldin, Phys. Rev. B 69 (2004) 125201.
[17] M.J. Calderon, S. Das Sarma, Ann. Phys. 322 (2007) 2618–2634.
[18] M. Khalid, A. Setzer, M. Ziese, P. Esquinazi, D. Spemann, A. Pöppl, E. Goering, Phys. Rev. B 81 (2010) 214414.
[19] L.L. Balcells, J.I. Beltrán, C. Martínez-Boubeta, Z. Konstantinović, J. Arbiol, B. Martínez, Appl. Phys. Lett. 97 (2010) 252503.
[20] R. Krause-Rehberg, H.S. Leipner, Positron Annihilation in Semiconductors, Defect Studies (Springer Series in Solid-State Sciences vol. 127), Springer, Berlin, 1999.
[21] J. Toivonen, T. Hakkarainen, M. Sopanen, H. Lipsanen, J. Oila, K. Saarinen, Appl. Phys. Lett. 82 (2003) 1.

[22] J. Gebauer, F. Borner, R. Krause-Rehberg, T.E.M. Staab, W. Bauer-Kugelmann, G. Kogel, W. Triftshauser, P. Specht, R.C. Lutz, E.R. Weber, M. Luysberg, J. Appl. Phys. 87 (2000) 12.
[23] B.J. Kooi, A. van Veen, J.Th.M. De Hosson, H. Schut, A.V. Fedorov, F. Labohm, Appl. Phys. Lett. 76 (2000) 9.
[24] Z.Q. Chen, T. Sekiguchi, X.L. Yuan, M. Maekawa, A. Kawasuso, J. Phys.: Condens. Matter 16 (2004) S293-S299.
[25] Z.Q. Chen, A. Kawasuso, Y. Xu, H. Naramoto, X.L. Yuan, T. Sekiguchi, R. Suzuki, T. Ohdaira, Phys. Rev. B 71 (2005) 115213.
[26] Matteo Pesci, Federico Gallino, Cristiana Di Valentin, Gianfranco Pacchioni, J. Phys. Chem. C 114 (2010) 1350–1356.
[27] Fenggong Wang, Zhiyong Pang, Liang Lin, Shaojie Fang, Ying Dai, Shenghao Han, Phys. Rev. B 80 (2009) 144424.